# Photocatalytic, Sonocatalytic and Sonophotocatalytic Degradation of Rhodamine B using MWCNTs-ZnO nanophotocatalysts

M. Ahmad[1, 2*], E. Ahmed[1], Z.L. Hong[2**], W. Ahmed[3], A. Elhissi[3] and N. R. Khalid[1, 2]

[1] Department of Physics, Bahauddin Zakariya University, Multan 60800, Pakistan
[2]State Key Laboratory of Silicon Materials, Department of Materials Science & Engineering, Zhejiang University, Hangzhou 310027, China
[3]Institute of Nanotechnology and Bioengineering, University of Central Lancashire, School of Medicine and Dentistry and School of Pharmacy and Biomedical Sciences, Preston PR1 2HE, United Kingdom

** Corresponding author. Mukhtar Ahmad*
*E-mail address: mzkhm73@gmail.com*
*Tel.: +92 61 9210091; fax: +92 61 9210098.*

*** Corresponding author. Zhanglian Hong*
*E-mail address; hong_zhanglian@zju.edu.cn*
*Tel./fax: +86 571 87951234.*

## Abstract

A series of ZnO nanoparticles decorated on multi walled carbon nanotubes (MWCNTs-ZnO) was synthesized using a facile solvothermal method. The intrinsic characteristics of as-prepared nanocomposites were studied using a variety of techniques including powder X-Ray diffraction (XRD), high resolution transmission electron microscope (HRTEM), transmission electron microscope (TEM), scanning electron microscope (SEM) with energy dispersive X-ray analysis (EDX), surface area analyzer (BET) and X-ray photoelectron spectroscopy (XPS). Optical properties studied using UV-Visible diffuse reflectance spectroscopy confirmed that the absorbance of ZnO increased in the visible-light region with the incorporation of MWCNTs. In this study, degradation of Rhodamine B (RhB) as a dye pollutant was investigated in the presence of pristine ZnO nanoparticles and MWCNTs-ZnO nanocomposites using photocatalysis and sonocatalysis systems separately and simultaneously. The natural sunlight and low power ultrasound were used as an irradiation source. The experimental kinetic data followed the pseudo-first order model in both photocatalytic and sonophotocatalytic processes but the rate constant of sonophotocatalysis is higher than it at photocatalysis process. The sonophotocatalysis was always faster than the respective individual processes due to the more formation of reactive radicals as well as the increase of the active surface area of MWCNTs-ZnO photocatalyst. Chemical oxygen demand (COD) of textile wastewater was measured at regular intervals to evaluate the mineralization of wastewater.

**Keywords:** ZnO, Rhodamine B, carbon nanotube, ultrasound, sonocatalysis

## 1. Introduction

The wastewaters discharged from textile and dyestuff industries cause serious environmental problems by destroying various life forms and consume dissolved oxygen owing to its strong color, a large amount of suspended solids, highly fluctuating pH as well as high temperature. Synthetic dyes are generally used in numerous manufacturing industries such as paper printing, textile dyeing, cosmetics and pharmaceuticals. About 20% of the total world production of dyes is lost during the dyeing processes **[1-2].** Rhodamine B is widely used in industrial purposes and capable to cause irritation to the skin, eyes, gastrointestinal tract as well as respiratory tract **[3].** Therefore, treatment of dye-containing effluents, i.e. Rhodamine B is a topic of significant interest among researchers. Color is one of the vital characteristics of these effluent streams and seems to be the most undesired, as it affects the nature of water by inhibiting sunlight penetration hence reducing photosynthetic action. Thus, color removal from industrial effluents has become a major concern in wastewater treatment, and treatment is needed before discharging to receiving water. For the removal of dye pollutants, various conventional methods such as adsorption on activated carbon, ultrafiltration, reverse osmosis, coagulation by chemical agent etc. can generally be used efficiently **[4-7].** Nevertheless, they are nondestructive methods, since they just transfer organic compounds from waste water to another phase, thus causing secondary pollution easily. Due to the large numbers of aromatic compounds present in dye molecules and stability of modern dye, the conventional treatment methods are ineffective for decolorization and mineralization **[8].**

Over the past several years, continuing interest has been focused on the application of advanced oxidation processes (AOP's) for the treatment of hazardous organic pollutants in water. Of the various AOP's commonly used for wastewater treatment, which has been paid to the use of

ultrasound as one of the effective technologies. **[9-10].** In 1894, the effects of ultrasound waves were first observed and when researchers irradiated water with ultrasound, they discovered that heat generated from the cavity implosion degrades water ($H_2O$) into extremely reactive hydrogen atoms ($H^{\bullet}$) and hydroxyl radicals ($OH^{\bullet}$) **[11].** Cavity implosion caused localized temperatures and pressures inside the bubble to touch the values of several thousand Kelvin and several hundred atmospheres, respectively **[12].**

Chemical reactions with $OH^{\bullet}$ from cavitation bubbles are referred to as sonochemical reactions which are promising for novel method of environmental processing such as waste water treatment. Photocatalytic degradation of organic compounds has also generated great interest for its potential to eliminate the hazardous chemical substances in water **[13-14].** A number of studies have demonstrated that the complete mineralization, i.e., oxidation to $CO_2$ and $H_2O$, of a variety of chlorinated aromatics occurred via heterogeneous photooxidation over $TiO_2$ and ZnO **[15-16].** For the degradation mechanisms of photocatalysis, a number of studies have indicated that $OH^{\bullet}$ was formed on photocatalyst during the photochemical reactions. Thus the combination of photocatalytic and ultrasonic irradiation, i.e. the so-called sonophotocatalysis seems to enhance the degradation ratio of organic pollutants due to the increase in the generation of $OH^{\bullet}$. In fact, the sonophotocatalysis has been reported to have a positive effect on the degradation ratio of the hazardous chemical substances **[17-19].** Among the results of these studies, ultrasound was shown to have a synergistic effect on the photodegradation of salicylic acid and formic acid **[18]**, while the detailed mechanisms have not been clarified yet. Recent observations have indicated that $TiO_2$ particles can enhance the oxidizing power of ultrasound even in the absence of ultraviolet irradiation **[20-21].** Although the application of heterogeneous catalysts in an ultrasonic system has been reported previously, $TiO_2$ was found to have a higher oxidizing

power and a specific mode of action in this system **[22-23].** The presence of a heterogeneous catalyst seems to increase the rate of formation of cavitation bubbles by providing additional nuclei **[24-25]**, which increase the pyrolysis of $H_2O$ molecules and formation of $OH^{\bullet}$. These observations may propose the possibility that ultrasonic irradiation over a $TiO_2$ catalyst enhances the generation of $OH^{\bullet}$, and this effect is mediated by mechanisms similar to those of $TiO_2$ photocatalysis.

In an effort to find an effective way for enhancing the efficiency of the ultrasonic-based degradation of organic pollutants with lower cost, we will apply ultrasonic irradiation together with addition of MWCNT-ZnO nanocomposite. The aim of this work was to study the degradation of RhB by means of sonocatalysis, photocatalysis and their combined application, sonophotocatalysis, concerning the effect of key operating conditions on the kinetics of dye conversion, sample mineralization and ecotoxicity. The particular interest in this work is to develop the suitable catalyst to be added in order to obtain the best degradation rate of RhB dye compounds from aqueous solutions. The characteristics and process behavior of MWCNT-ZnO nanocomposite will be determined by various characteristics test. In addition, the priority will be investigating the effectiveness of the MWCNT-ZnO nanocomposite against the degradation of RhB dye compounds from aqueous solutions.

## 2. Experimental

### 2.1. Materials

MWCNTs used as the support material for the preparation of MWCNTs-ZnO nanocomposites were purchased from Beijing Chemical Company China and used without further purification. Other chemical reagents, such as zinc acetate ($Zn(CH_3COO)_2 \cdot 2H_2O$), diethyleneglycol (DEG),

absolute ethanol supplied by Sinopharm Chemical Reagent Company China were analytical grade and used without further purification.

### 2.2. Preparation of ZnO, MWCNTs-ZnO nanocomposites

MWCNTs-ZnO nanocomposites were synthesized using a solvothermal method based on Zhu's work with modifications **[26].** The synthesis process of MWCNTs-ZnO nanocomposites comprises two steps. In the first step, 2.20 g zinc acetate was dissolved in 500 mL DEG. Subsequently, 20 mL deionized water was added into the above prepared solution. Afterwards, the mixture was magnetically stirred at 160–180 ˚C for 10 min and then placed in air for 2 h to form aged homogeneous ZnO sol. In the second step, certain amount of purified MWCNTs was dispersed into the above sol with ultrasonication for 30min. After that, the solution was slowly heated to 160–180 ˚C with vigorous magnetic stirring for 2 h. After being cooled to the room temperature, MWCNTs-ZnO nanocomposites were obtained after centrifuging, washing by absolute ethanol and deionized water several times and drying the suspension at 80 ˚C for 24 h. For comparison, pure ZnO were prepared via solvothermal route under the same conditions. The codes of the composite samples are listed in **Table 1.**

### 2.3. Characterization

The phase purity of the products were characterized using an automated X-ray powder diffractometer (XRD, PANalytical Empyrean) with Cu Kα as radiation source (λ=0.15406 nm). The surface morphology, particle size and composition of photocatalysts were examined using a scanning electron microscope (SEM, HITACHI S-4800 combined with EDX), transmission electron microscope (TEM, JEOL JEM 1200EX), high resolution transmission electron microscope (HR-TEM, FEI TECNAI $G^2$ F20) and X-ray photoelectron spectroscopy (XPS, VG ESCALAB MARK II, with a monochromatic Mg Kα X-ray source). BET specific surface areas

of the samples were determined using a Surface Area Analyzer (NOVA 2200e Quantachrome, USA) using nitrogen as a purge gas. The UV-vis absorption spectra were measured under the diffuse reflectance mode in the range of 300-800 nm using a HITACHI U-4100 UV-vis spectrophotometer with an integrating sphere accessory. Photoluminescence (PL) emission spectra were recorded using a HITACHI F-4500 Fluorescence spectrophotometer. The samples were excited with a 325 nm wavelength light at room temperature and the emission scanned between 360-560 nm.

**2.4. Photocatalytic, Sonocatalytic and Sonophotocatalytic activity**

The sonocatalytic and Sonophotocatalytic degradation of RhB model dye was estimated by ZnO and MWCNTs-ZnO catalysts with ultrasonic bath, operated with a fixed frequency of 35 kHz. The reactions were carried out in an open cylindrical stainless glass vessel covered with transparent plastic sheet. The photocatalytic degradation was also tested by ZnO and MWCNTs-ZnO photocatalysts and an aqueous solution of RhB in a same glass vessel and irradiation system with sunlight. In each experiment, 30 mg photocatalyst was suspended in 30 mL model dye aqueous solution with a concentration of 20 mg/L. Then, the suspended solution was placed in the dark for at least 30 min to establish adsorption-desorption equilibrium. Experiments were then carried out under natural sunlight, ultrasonic irradiation and natural sunlight-ultrasonic irradiation respectively. The temperature of the suspension was kept at about 20 $^{o}$C using an external cooling jacket with recycled water. After every 30 min, 3 mL suspension was sampled, centrifuged immediately and the supernatant evaluated using a UV-Vis. absorption spectrometer. The pink color of the solution faded gradually with time due to the adsorption and degradation of RhB. The intensity of the main absorption peak of the model dye was referred to as a measure of

the residual dye concentration. Finally, the degree of degradation is expressed by $C_t/C_o$, which is the ratio of the temporal dye concentration to the initial dye concentration.

### 2.5. Analytical method

The total organic carbon (TOC) content was measured after the degradation of RhB model dye in the presence of the photocatalysts under sunlight irradiation **[27].** The decrease in the carbon content indicates the degradation of the organic dye into nontoxic decomposition compounds. The mineralization of textile industry waste water was determined by measuring the decrease of chemical oxygen demand (COD) of the waste water. COD of textile mill effluent was estimated before and after the photocatalytic treatment with a standard dichromate method using COD digester. As-received effluent (COD = 4987 $mgL^{-1}$) was suitably diluted in order to facilitate light penetration through solution and the initial COD of diluted effluent was 627 $mgL^{-1}$. The percentage photodegradation efficiency (η) was calculated from the following expression

$$\eta = [(COD_{initial} - COD_{final}) / COD_{initial}] \times 100 \ldots\ldots\ldots (1)$$

All the experiments were performed under the identical experimental conditions such as sunlight irradiation (between 10 am and 4 pm during summer season), constant temperature, pH and photocatalyst load etc.

## 3. Results and discussion

XRD analysis measurements were employed to investigate the composition and structure of the synthesized samples. Fig. 1a depicts the typical XRD patterns of the powdered MWCNTs, ZnO and the MWCNTs-ZnO nanocomposite. For MWCNTs, the peaks at the angle $2\theta = 25.7^\circ$ and $42.9^\circ$ were associated with the (0 0 2), (1 0 0) diffractions of the hexagonal graphite structure **[28].** For MWCNTs-ZnO nanocomposite, diffractions of both MWCNTs and ZnO could be observed. The main dominant peaks for ZnO were identified at $2\theta = 31.7^\circ$, $34.4^\circ$, $36.2^\circ$, $47.5^\circ$,

56.6◦, 62.8◦ and 67.9◦; which can be indexed as (1 0 0), (0 0 2), (1 0 1), (1 0 2), (1 0 2), (1 0 0) and (1 0 3) associated to the diffractions of the hexagonal wurtzite phase **[29].** XRD results of ZnO showed prominent (1 0 0), (0 0 2) and (1 0 1) reflections among which (1 0 1) is of highest intensity. The average crystallite size of ZnO in MWCNTs-ZnO nanocomposite can be roughly estimated using the Debye-Scherer formula for spherical crystallites and the estimated size was around 17-35 nm. EDX was carried out to probe the composition of the ZnO, MCZ-3 and MCZ-4 nanocomposites. Fig. 2 represents the EDX spectra of the samples. It reveals the presence of Zn, O and C on the surface of the nanotubes, which confirms the existence of ZnO nanoparticles on MWCNTs consistent with the results of XRD. The C signal originates from MWCNTs and there is no unexpected elements being detected, indicating the purity of the samples. The values of BET surface area of pure ZnO and MWCNTs-ZnO nanocomposites are presented in **Table 2.** As the results shown, the BET surface areas of pristine ZnO and MWCNTs were 31.4 and 227.3 $m^2/g$, respectively. It can be seen that, the specific surface areas gradually increase with the increasing MWCNTs content, which enhances the photocatalytic performance.

The direct evidence of the formation of ZnO nanoparticles on the surface of MWCNTs is given by SEM, TEM and HRTEM in Fig. 3. Fig. 3a showed the SEM image of ZnO nanoparticles, it is clear that the particles are well dispersed and homogenous. The morphological characterization of the MCZ-5 catalyst is presented in Fig. 3(b-c). It was observed that MWCNTs is covered with ZnO nanoparticles. These homogenous ZnO nanoparticles were uniformly dispersed on MWCNTs surface and some small bundles were found with irregular agglomerate dispersion. It was well explained that the good dispersion of small particles were not well homogenized during the vigorous stirring. TEM images of ZnO, MCZ-4 and MCZ-5 catalysts are shown in Fig. 3(d-h). The TEM image (Fig. 3d) clearly show that the particles are dispersed, homogenous and

having good agreement with the results given by Scherer formula. Fig. 3(e-h) show that all of the MWCNTs were covered with a dense layer of ZnO nanoparticles and no free MWCNT were found. HR-TEM image (Fig. 3i) shows better view with higher magnification of the sample MCZ-5. The ZnO nanoparticles deposited on MWCNT surface showed a strong interphase structure and the particle size was uniform, which indicated that ZnO nanoparticles can be dispersed tightly on the surface of MWCNT. The binding between ZnO and MWCNT surface is tight enough to resist repeated ultrasonication processes.

The light-absorbance properties were characterized using UV-Vis spectroscopy and diffuse reflectance spectra of the as-synthesized MCZ-1, MCZ-2, MCZ-3, MCZ-4 and MCZ-5 nanocomposites, together with pure ZnO for comparison are shown in Fig.4a. The absorption spectra have been obtained from reflectance data using the Kubelka-Munk algorithm are shown in Fig.4b. It is observed that the absorbance of the MWCNTs-ZnO nanocomposites has increased even in visible light region with the increase of CNT content, which is similar to findings of previous reports that evaluated CNT/ZnO nanocomposite synthesized via sol-gel reaction **[30].** The presence of MWCNTs in nanocomposite induces the increased visible light absorption intensity, which may be due to the increase of surface electric charge of the oxides in the ZnO/graphene composite and the modification of the fundamental process of electron–hole pair formation during irradiation [**31**]. The results demonstrate the significant influence of MWCNTs on the optical properties, suggesting that incorporation of MWCNTs enhances the visible-light absorption and is expected to improve the visible-light photocatalytic activity.

Fig. 5 shows the photoluminescence (PL) emission spectra of as-synthesized ZnO, MCZ-1, MCZ-2, MCZ-3, MCZ-4 and MCZ-5 nanocomposites. The spectra exhibited a broad emission band in the range of 380 to 500 nm, which was ascribed to luminescence from localized surface

states due to recombination of photogenerated electron–hole pairs **[32].** Since ZnO is a good electron donor and carbon materials are relatively good electron acceptors, the synergistic effect between these two components would effectively reduce recombination and lead to an increased charge carrier separation **[33].** The PL intensity decreases with increasing the MWCNTs content. It is well known that the PL emission is due to the recombination of excited electrons and holes; the lower PL intensity may indicate the lower recombination rate of electrons and holes under light illumination. ZnO has highest PL intensity amongst all of the samples indicating a high probability recombination of electrons and holes. The emission intensity significantly decreases with the graphene introduction, implying that the recombination of photogenerated carriers was effectively suppressed. Amongst all the samples the lowest emission intensity was observed for MCZ-5 nanocomposite, suggesting that the recombination of photogenerated carriers is suppressed due to the effect of graphene.

XPS is a surface sensitive technique that probes the electrons ejected from the surface of samples. For information about oxidation states of ions in our sample XPS was performed on the MCZ-4 nanocomposite. The obtained data were calibrated by using the adventitious carbon at a binding energy of 284.6 eV. The survey spectrum (Fig. 6a) indicates that the sample is composed of Zn, O and C, and no peaks of other elements were observed. The deconvoluted C 1s XPS spectrum (Fig. 6b) shows three peaks at 284.8, 286.7 and 288.7 eV. The binding energy at 284.8 eV is assigned to the C–C bond ($sp^2$) of graphene. The peak at 286.7 eV is ascribed to the C–O bond, while the peak at 288.7 eV is assigned to the C = C bond **[34]**. XPS spectra of O1s shown in Fig. 6c are asymmetric, indicating that multi-component oxygen species are present in the surface. The curve was deconvoluted by Gaussian fittings in to two separate peaks ‘α’ and ‘β’ located at 530.0 eV, 531.5eV, respectively. The peak located at 530.0 eV may be attributed to the Zn–O

crystal lattice oxygen. The higher energy peak located at 531.5eV can be associated with chemisorbed oxygen caused by the surface hydroxyl **[35]**. Fig. 6d spectra of the $Zn2p^{3/2}$ and $Zn2p^{1/2}$ exhibits asymmetric peaks located at 1022.6 eV and 1045.6 eV which fitted nicely to Gaussian peaks, ruling out the possibility of existence of multiple components of Zn in our sample **[36]**.

To determine and compare the photocatalytic, sonocatalytic and sonophotocatalytic efficiencies of ZnO nanoparticles, pristine MWCNTs and MWCNTs-ZnO nanocomposites, a series of experiments were conducted using RhB dye as test contaminant. The degradation profiles of RhB dye, photocatalysed by ZnO nanoparticles, MWCNTs and MWCNTs-ZnO nanocomposites under sunlight irradiations are shown in Fig. 7a. It is observed that RhB was hardly reduced even after exposure for 60 min to the sunlight in absence of the photocatalyst. It was also observed that MWCNTs-ZnO nanocomposites exhibited better photocatalytic performance than that of ZnO and MWCNTs. The removal rate of RhB for ZnO and MWCNTs was only 26% and 24% respectively. By contrast, when carbon nanotubes were introduced into ZnO, the removal rate was increased to 37%, 45%, 67%, 86% and 89% for MCZ-1, MCZ-2, MCZ-3, MCZ-4 and MCZ-5 respectively. We consider MCZ-4 as better photocatalyst than MCZ-5 because it has almost the same removal efficiency as that of MCZ-5 but utilized half amount of MWCNTs. These findings indicate that the introduction of graphene into ZnO plays an important role in the photocatalytic performance of the MWCNTs-ZnO nanocomposites. Photocatalytic reactions on the MWCNTs-ZnO nanocomposites surface can be expressed by the Langmuir-Hinshelwood model **[37].** The photocatalytic degradation of RhB by the MWCNTs-ZnO nanocomposites under sunlight obeyed pseudo-first order kinetics with respect to the concentration of RhB:

$$ln(C_o/C_t) = K_{photo} \times t$$

where $K_{photo}$ is the apparent reaction rate constant for photocatalysis, used as the basic kinetic parameter for different photocatalysts; $C_o$ is the initial concentration of RhB in aqueous solution at time t = 0; and $C_t$ is the residual concentration of RhB at time t. The apparent reaction rate constant values could be deduced from the linear fitting of $ln(C_o/C_t)$ versus $t$. The apparent reaction rate constant for different catalysts was studied and the results are presented in Fig. 8a. The results show that $K_{photo}$ was enhanced by the introduction of graphene. The high photocatalytic activity of the nanocomposites might be attributed to the result of strong coupling between ZnO and MWCNTs.

Photocatalytic degradation of dyes in the presence of ZnO nanoparticles and MWCNTs-ZnO nanocomposites has been reported in several papers **[26,38].** The basic mechanism of photocatalysis involves photo excitation of electrons from the valence band to the conduction band of a wide band gap semiconductor photocatalyst leaving a positive hole in the valence band **[39-40].** The as-formed charge carriers (electrons and holes) at catalyst surface initiate redox reactions in the adsorbed molecules prior to annihilation of the exciton, thus removing or reducing contaminating molecules.

An interesting alternative to the photocatalytic degradation of pollutants in waste water is sonocatalysis **[41].** The effect of ultrasonic irradiation on RhB degradation by the ZnO nanoparticles and MWCNTs-ZnO nanocomposite catalyst were investigated, in depicted in Fig. 7b. The ability of ultrasound, MWCNTs, ZnO nanoparticles, and MWCNTs-ZnO nanocomposites to degrade RhB was compared. It is observed that after adsorption for 30 min followed by ultrasonic irradiation for 60 min, MCZ-5 has degraded the most RhB (93%), whereas ZnO, MWCNTs, MCZ-1, MCZ-2, MCZ-3, MCZ-4 and ultrasonic irradiation alone degraded 30%, 27%, 42%, 52%, 71%, 89% and 3% of RhB, respectively. The sonocatalytic

degradation of RhB by the MWCNTs-ZnO nanocomposites obeyed pseudo-first order kinetics with respect to the concentration of RhB:

$$ln(C_o/C_t) = K_{sono} \times t$$

The apparent reaction rate constant for sonocatalysis ($K_{sono}$) determined for the different catalysts under ultrasonic irradiations are presented in Fig. 8b. The results show that $K_{sono}$ was enhanced by the introduction of MWCNTs. The degradation rate of RhB in the presence of pristine ZnO and MWCNTs was lower than that with the MWCNTs-ZnO nanocomposites. As clearly seen, sonocatalytic degradation occurs appreciably faster than photocatalytic degradation under similar experimental conditions. Sonocatalytic degradation of dyes in the presence of different catalysts has been reported in several papers and the oxidation process of dyes is dependent on OH· **[42-43],** and can be explained by the well-known mechanism of hot spots and sonoluminescence as follows. First, the formation of cavitation bubbles can be increased by the heterogeneous nucleation of bubbles, generating hot spots in the solution. These hot spots can cause $H_2O$ molecules to pyrolyze to form OH·. Second, sonoluminescence involves intense UV light, which excites the catalyst particles to act as photocatalysts during sonication. Usually sonochemical reaction pathways to degrade organic compounds involve the sonolysis of water as the solvent inside collapsing cavitation bubbles under extremely high temperature and pressure **[43-44].** When a catalyst is also added, ultrasonic irradiation not only induces sonolysis of water but also couples with the catalyst to produce electron-hole pairs. The electron-hole pairs can produce OH· radicals and superoxide anions $\cdot O_2^-$, which can decompose dyes to $CO_2$, $H_2O$, and inorganic species.

Also, the catalytic activity of the MWCNTs-ZnO nanocomposites is mainly enhanced compared with that of ZnO by the high efficiency of charge separation through the synergistic effect of

MWCNTs and ZnO. The improved ability of the MWCNTs-ZnO nanocomposites to adsorb RhB compared with that of ZnO can be ascribed to larger surface area. MWCNTs act as an electron acceptor from ZnO, significantly hindering the recombination of charge carriers and thus improving catalytic activity.

In further experiments, RhB degradation by means of simultaneous ultrasound and sunlight irradiation in the presence of ZnO and MWCNTs-ZnO nanocomposites was studied. The temporal changes in RhB concentration during sonophotocatalysis at initial concentration and various catalyst loadings are shown in Fig. 7c. Like photocatalysis and sonocatalysis, sonophotocatalysis also appear to follow a pseudo-first order kinetic expression

$$ln(C_o/C_t) = K_{sonophoto} \times t$$

The apparent reaction rate constant for sonophotocatalysis ($K_{sonophoto}$) are summarized in Fig. 8c. As seen from Fig. 8, sonophotocatalytic degradation generally occurs faster than that during the respective individual processes at similar operating conditions. Interestingly, there appears to be a synergistic effect between ultrasound and sunlight irradiation in the presence of ZnO and MWCNTs-ZnO nanocomposites since reaction rate constant of the combined process is greater than that of the rate constants of the individual processes.

The beneficial effect of coupling photocatalysis with sonolysis may be attributed to several reasons, namely: (i) increased production of hydroxyl radicals in the reaction mixture (ii) enhanced mass transfer of organics between the liquid phase and the catalyst surface **[2]**, (iii) catalyst excitation by ultrasound-induced luminescence which has a wide wavelength range below 375 nm **[42,46]** and (iv) increased catalytic activity due to ultrasound de-aggregating catalyst particles, thus increasing surface area **[47]**.

The total organic carbon (TOC) content was measured before and after the degradation of RhB organic dye in the presence of the photocatalysts, sonocatalysts and sonophotocatalysts under sunlight, ultrasonic and sunlight-ultrasonic irradiations, respectively. After degradation the TOC content of model dye decreased with time (Fig. 9). The decrease in the carbon content indicates the degradation of the RhB dye into nontoxic compounds.

During textile manufacturing processes huge amount of waste water containing dyestuffs with intensive colour and toxicity is introduced into the aquatic system. An effluent of this type has been considered for this photocatalytic degradation study. COD removal efficiencies of the effluent by pristine ZnO and MWCNTs-ZnO nanocomposites photocatalysts under the sunlight irradiation are shown in Fig. 10. COD reduction confirms the destruction of the organic molecules in the effluents along with colour removal. The differences in the COD values for different samples are probably due to the different adsorption capacity and photocatalytic activity as mentioned above. Similar to the experimental results on the degradation of RhB, MCZ-5 showed the best removal efficiency. This may be due to the photocatalytic reactions that occur on the surface of the composite catalyst.

The stability of MCZ-4 nanocomposite as catalyst under sunlight and ultrasonic irradiations was also studied (Fig. 11). It can be seen that the photocatalytic and sonocatalytic activity of composite did not decrease conspicuously after five successive cycles of degradation tests, indicating that the composite was fairly stable under the conditions used in this study.

**4. Conclusions**

MWCNTs-ZnO nanocomposite was prepared *via* a simple solvothermal method, using diethylene glycol as a solvent and a reducing agent. The SEM, TEM and HR-TEM show that the ZnO nanoparticles were randomly anchored onto the multi-walled carbon nanotubes. The

interactions of ZnO with multi-walled carbon nanotubes were investigated further using BET, XPS, PL and DRS measurements. It was found that all MWCNTs-ZnO nanocomposites have stronger light absorption in visible light region than pure ZnO. The as-prepared nanocomposite exhibited enhanced photocatalytic, sonocatalytic and sonophotocatalytic activity in degrading RhB dye compared with the ZnO nanoparticles and multi-walled carbon nanotubes, which can be attributed to enhance the electron-holes separation at the hetero-interface and the formation of more reactive radicals as well as the increase of the active surface area. COD reduction of textile waste water confirms the destruction of the organic molecules in the effluents with colour removal. MCZ-4 composite also shows a superior stability according to the cycling tests. Therefore, the MWCNTs-ZnO nanocomposites are excellent candidates for applications in a number of environmental issues.

## Acknowledgments

M. Ahmad is gratefully acknowledged the financial support from Higher Education Commission (HEC) of Pakistan for IRSIP scholarship. This work was supported partially by Natural Science Foundation of China (No. 51072180), the Fundamental Research Funds for the Central Universities (No. 2009QNA4005), and the State Key Laboratory of Silicon Materials (SKL2009-14) at Zhejiang University.

**References**


[1] E. Sayan, M. E. Edecan, An optimization study using response surface methods on the decolorization of Reactive Blue 19 from aqueous solution by ultrasound, Ultrason. Sonochem.15 (2008) 530–538.

[2] M. Mrowetz, C. Pirola, E. Selli, Degradation of organic water pollutants through sonophotocatalysis in the presence of $TiO_2$, Ultrason. Sonochem. 10 (2003) 247–254.

[3] S. Merouani, O. Hamdaoui, F. Saoudi, and M. Chiha, Sonochemical degradation of Rhodamine B in aqueous phase: effects of additives, J. Eng. Chem. 158 (2010) 550–557.

[4] A. Houas, H. Lachheb, M. Ksibi, E. Elaloui, C. Guillard, J.M. Hermann, Photocatalytic degradation pathway of methylene blue in water, Appl. Catal. B: Environ. 31 (2001) 145–157.

[5] M. Saquib, M. Muneer, Titanium dioxide mediated photocatalysed degradation of a textile dye derivative, acid orange 8, in aqueous suspensions, Desalination 155 (2003) 255–263.

[6] W.Z. Tang, H. An, Photocatalytic oxidation of commercial dyes in aqueous solutions, Chemosphere 31 (1995) 4157–4170.

[7] V. Meshko, L. Markovska, M. Mincheva, A.E. Rodrigues, Adsorption of basic dyes on granular activated carbon and natural zeolite, Wat. Res. 35 (2001) 3357–3366.

[8] W.S. Kuo, P.H. Ho, Solar photocatalytic decolorization of methylene blue in water, Chemosphere 45 (2001) 77–83.

[9] J. Berlan, F. Trabelsi, H. Delmas, A.M. Wilhelm, J.F. Petrignani, Oxidative degradation of phenol in aqueous media using ultrasound, Ultrason. Sonochem. 1 (1994) 97-102.

[10] P.R. Gogate, Cavitation: an auxiliary technique in wastewater treatment schemes Adv. Environ. Res. 6 (2002) 335-358**.**

[11] K.S. Suslick, The Chemical effects of ultrasound, Sci. Am. 260 (1989) 80-86.

[12] K.S. Suslick, D.A. Hammerton, R.E. Cline Jr., The sonochemical hot spot, J. Am. Chem. Soc. 108 (1986) 5641-5642.

[13] M.A. Fox, M.T. Dulay, Heterogeneous photocatalysis, Chem. Rev. 93 (1993) 341-357.

[14] M.R. Hoffmann, S.T. Martin, W. Choi, D.W. Bahnemann, Environmental applications of semiconductor photocatalysis, Chem. Rev. 95 (1995) 69-96.

[15] S. Tunesi, M.A. Anderson, Photocatalysis of 3,4-DCB in $TiO_2$ Aqueous suspensions; Effects of temperature and light intensity; CIR-FTIT Interfacial Analysis, Chemosphere 16 (1987) 1447-1456.

[16] M. Ahmad, E. Ahmed, Z.L. Hong, J.F. Xu, N.R. Khalid, A. Elhissi, W. Ahmed, A facile one-step approach to synthesizing ZnO/graphene composites for enhanced degradation of methylene blue under visible light, Appl. Surf. Sci. 274 (2013) 273-281.

[17] I.Z. Shirgaonkar, A.B. Pandit, Sonophotochemical destruction of aqueous solution of 2, 4, 6-trichlorophenol, Ultrason. Sonochem. 5 (1998) 53-61.

[18] L. Davydov, E.P. Reddy, P. France, P.G. Smirniotis, Sonophotocatalytic destruction of organic contaminants in aqueous systems on $TiO_2$ powders Appl. Catal. B: Environ. 32 (2001) 95-105.

[19] A.B. Pandit, P.R. Gogate, S. Mujumdar, Ultrasonic degradation of 2: 4: 6 trichlorophenol in presence of $TiO_2$ catalyst, Ultrason. Sonochem. 8 (2001) 227-231.

[20] M. Kubo, K. Matsuoka, A. Takahashi, N. Shibasaki-Kitakawa, T. Ynemoto, Kinetics of ultrasonic degradation of phenol in the presence of $TiO_2$ particles, Ultrason. Sonochem. 12 (2005) 263-269.

[21] J. Wang, B. Guo, X. Zhang, Z. Zhang, J. Han, J. Wu, Sonocatalytic degradation of methyl orange in the presence of $TiO_2$ catalysts and catalytic activity comparison of rutile and anatase, Ultrason. Sonochem. 12 (2005) 331-337.

[22] N.H. Ince, R. Belen, Aqueous phase disinfection with power ultrasound: process kinetics and effect of solid catalysts, Environ. Sci. Technol. 35 (2001) 1885-1888.

[23] M.D. Farshbaf, C. Ogino, S. Matsumura, N. Shimizu, Kinetics of disinfection of Escherichia coli by catalytic ultrasonic irradiation with $TiO_2$, Biochem. Eng. 9. 25 (2005) 243-248.

[24] H. Sekiguchi, Y. Saita, Effect of alumina particles on sonolysis degradation of chlorobenzene in aqueous solution, J. Chem. Eng. Jpn. 34 (2001) 1045-1048.

[25] T. Tuziuti, K. Yasui, M. Sivakumar, Y. Iida, Correlation between acoustic cavitation noise and yield enhancement of sonochemical reaction by particle addition, J. Phys. Chem. A 109 (2005) 4869-4872.

[26] L.P. Zhu, G.H. Liao, W.Y. Huang, L.L. Mac, Y. Yang, Y. Yu, S.Y. Fu, Preparation, characterization and photocatalytic properties of ZnO-coated multi-walled carbon nanotubes, Mater. Sci. Eng. B 163 (2009) 194-198.

[27] D. Mukherjee, Development of a novel $TiO_2$-polymeric film photocatalyst for water purification both under UV and solar Illuminations, Ph.D. Thesis (2011) 143-144.

[28] T.A. Saleh, M.A. Gondal, Q.A. Drmosh, Z.H. Yamani, A. AL-yamani, Enhancement in photocatalytic activity for acetaldehyde removal by embedding ZnO nano particles on multiwall carbon nanotubes, Chem. Eng. J. 166 (2011) 407–412.

[29] H.F. McMurdie, M.C. Morris, E.H. Evans, B. Paretzkin, W. Wong-Ng, L. Ettlinger, C.R. Hubbard, Standard X-ray diffraction powder patterns from the JCPDS research associateship, Powder Diffr. 1 (1986) 64–77.

[30] X. Wang, S. Yao, X. Li, Sol-gel preparation of CNT/ZnO nanocomposite and its photocatalytic property, Chin. J. Chem. 27 (2009) 1317-1320.

[31] T.G. Xu, L.W. Zhang, H.Y. Cheng, Y.F. Zhu, "Significantly enhanced photocatalytic performance of ZnO via graphene hybridization and the mechanism study," Chem. Reviews, 101 (2010) 382-387.

[32] J. Ki-Seok, O. Seung-Do, Y.D. Suh, H. Yoshikawa, H. Masuhara, M. Yoon, "Blinking photoluminescence properties of single $TiO_2$ nanodiscs: Interfacial electron transfer dynamics," J. Phys. Chem. Chem. Phy. 11 (2009) 534–542.

[33] J.L. Wu, X.P. Shen, L. Jiang, K. Wang, K.M. Chen, "Solvothermal synthesis and characterization of sandwich-like graphene/ZnO nanocomposites," Appl. Surf. Sci. 256 (2010) 2826-2830.

[34] L. Ai, C. Zhang, Z. Chen, "Removal of methylene blue from aqueous solution by a solvothermal synthesized graphene/magnetite composite" J. Hazard. Mater. 192 (2011) 1515– 1524.

[35] B. Wang, Y. Wang, J. Park, H. Ahn, G. Wang, In situ synthesis of $Co_3O_4$/Graphene nanocomposite material for lithium Ion batteries and supercapacitors with high capacity and supercapacitance, J. Alloy. Compd. 509 (2011) 7778–7783.

[36] R.K. Singhal, M.S. Dhawan, S.K. Gaur, S.N. Dolia, S. Kumar, T. Shripathi, U.P. Deshpande, Y.T. Xing, E. Saitovitch, K.B. Garg, Room temperature ferromagnetism in

Mn-doped dilute ZnO semiconductor: An electronic structure study using X-ray photoemission, J. Alloy. Compd. 477 (2009) 379–385.

[37] Y. Li, X. Li, J. Li, J. Yin, Photocatalytic degradation of methyl orange by $TiO_2$-coated activated carbon and kinetic study, Wat. Res. 40 (2006) 1119.

[38] M. Ahmad, Z.L. Hong, E. Ahmed, N.R. Khalid, A. Elhissi, W. Ahmad, Effect of fuel to oxidant molar ratio on the photocatalytic activity of ZnO nanopowders, Ceram. Int. 39 (2013) 3007–3015.

[39] M. Ahmad, E. Ahmed, Yuewei Zhang, N.R. Khalid, J.F. Xu, M. Ullah, Z.L. Hong, Preparation of highly efficient Al-doped ZnO photocatalyst by combustion synthesis, Cur. Appl. Phys. 13 (2013) 697–704.

[40] M. Li, Z.L. Hong, Y.N. Fang, F.Q. Huang, Synergistic effect of two surface complexes in enhancing visible-light photocatalytic activity of titanium dioxide, Mater. Res. Bull. 43 (2008) 2179–2186.

[41] K. Okitsu, K. Iwasaki, Y. Yobiko, H. Bandow, R. Nishimura, Y. Maeda, Sonochemical degradation of azo dyes in aqueous solution: a new heterogeneous kinetics model taking into account the local concentration of OH radicals and azo dyes, Ultrason. Sonochem. 12 (2005) 255-262.

[42] N. Shimizu, C. Ogino, M.F. Dadjour, T. Murata, Sonocatalytic degradation of methylene blue with $TiO_2$ pellets in water, Ultrason. Sonochem. 14 (2007) 184-190.

[43] K. Zhang. W. Oh, Kinetic study of the visible light-induced sonophotocatalytic degradation of MB solution in the presence of Fe/$TiO_2$-MWCNT Catalyst, Bull Korean Chem. Soc. 31(2010) 1589-1595.

[44] J. Saien, H. Delavari, A.R. Soleymani, Sono-assisted photocatalytic degradation of styrene-acrylic acid copolymer in aqueous media with nano titania particles and kinetic studies. J. Hazard. Mater. 177 (2010) 1031-1038.

[45] N. Wang, L.H. Zhu, M.Q. Wang, D.L. Wang, H.Q. Tang, Sono-enhanced degradation of dye pollutants with the use of $H_2O_2$ activated by $Fe_3O_4$ magnetic nanoparticles as peroxidase mimetic, Ultrason. Sonochem. 17 (2010) 78-83.

[46] J. Wang, Z. Pan, Z. Zhang, X. Zhang, F. Wen, T. Ma, Y. Jiang, L. Wang, L. Xu, P. Kang, Sonocatalytic degradation of methyl parathion in the presence of nanometer and ordinary

anatase titanium dioxide catalysts and comparison of their sonocatalytic abilities, Ultrason. Sonochem. 13 (2006) 493-500.

[47] A.M.T. Silva, E. Nouli, A.C. Carmo-Apolinario, N.P. Xekoukoulotakis, D. Mantzavinos, Sonophotocatalytic/$H_2O_2$ degradation of phenolic compounds in agro-industrial effluents", Catal. Today 124 (2007) 232-239.

# Figure Captions

**Fig. 1.** (a) The XRD patterns of (1) pristine MWCNT; (2) ZnO nanoparticles; (3) MCZ-1; (4) MCZ-2; (5) MCZ-3; (6) MCZ-4 and (7) MCZ-5 nanocomposites (b) Comparison of peaks from the XRD patterns of MWCNT, ZnO nanoparticles and MCZ-5 nanocomposite

**Fig. 2.** EDX spectra of ZnO, MCZ-3 and MCZ-4 nanocomposite

**Fig. 3.** SEM images of (a) ZnO (b) MCZ-5; lower magnification (c) MCZ-5; higher magnification, TEM images of (d) ZnO (e) MCZ-5; lower magnification (f) MCZ-5; higher magnification (g) MCZ-4; lower magnification (h) MCZ-4; higher magnification, (i) HR-TEM image of MCZ-5 nanocomposite

**Fig. 4.** (a) UV-Vis diffuse reflectance spectra (%) and (b) Absorption spectra of (1) ZnO; (2) MWCNT (3) MCZ-1; (4) MCZ-2; (5) MCZ-3; (6) MCZ-4; (7) MCZ- 5 photocatalysts

**Fig. 5.** Room-temperature PL emission spectra of (1) ZnO; (2) MWCNT (3) MCZ-1; (4) MCZ-2; (5) MCZ-3; (6) MCZ-4; (7) MCZ- 5 photocatalysts with excitation wavelength of 325 nm

**Fig. 6.** (a) XPS survey spectra; high resolution spectra of (b) C 1s; (c) O 1s (d) Zn 2p of MCZ-4 nanocomposite

**Fig. 7.** Photocatalytic, Sonocatalytic and Sonophotocatalytic degradation of RhB in the presence of (1) without catalyst (2) ZnO (3) MWCNT (4) MCZ-1; (5) MCZ-2; (6) MCZ-3; (7) MCZ-4; (8) MCZ- 5 photocatalysts

**Fig. 8.** Photocatalytic, Sonocatalytic and Sonophotocatalytic apparent reaction rate constant in the presence of (1) without catalyst (2) ZnO (3) MWCNT (4) MCZ-1; (5) MCZ-2; (6) MCZ-3; (7) MCZ-4; (8) MCZ- 5 photocatalysts

**Fig. 9.** The $\ln(TOC_o/TOC_t)$ vs time curves of mineralization of RhB for Photocatalytic, Sonocatalytic and Sonophotocatalytic degradation in the presence of (1) without catalyst (2) ZnO (3) MWCNT (4) MCZ-1; (5) MCZ-2; (6) MCZ-3; (7) MCZ-4; (8) MCZ- 5 photocatalysts; $TOC_o$ and $TOC_t$ are the initial concentration and the reaction concentration of model dyes, respectively.

**Fig. 10.** COD values of textile industry waste water with different photocatalysts

**Fig. 11.** Recycle photocatalytic and Sonocatalytic degradation performance of MCZ-4 nanocomposite

**Table 1:** Code names of different samples

**Table 2:** BET specific surface area, reaction rate constant of photocatalytic degradation and half-life of various photocatalysts

# Table 1

| Sr. No. | Sample Name | Sample Code |
|---|---|---|
| 1 | ZnO | ZnO |
| 2 | 1 wt.% MWCNT-ZnO | MCZ-1 |
| 3 | 2 wt.% MWCNT-ZnO | MCZ-2 |
| 4 | 5 wt.% MWCNT-ZnO | MCZ-3 |
| 5 | 10 wt.% MWCNT-ZnO | MCZ-4 |
| 6 | 20 wt.% MWCNT-ZnO | MCZ-5 |

# Table 2

| Sample | BET Area ($m^2/g$) | $r_o$ ($10^2 mgL^{-1}min^{-1}$) | $t_{1/2}$ (min) |
|---|---|---|---|
| ZnO | 31.4 | 0.06 | 231 |
| MWCNT | 227.3 | 0.057 | 243 |
| MCZ-1 | 49.6 | 0.1 | 139 |
| MCZ-2 | 61.3 | 0.12 | 116 |
| MCZ-3 | 87.2 | 0.24 | 58 |
| MCZ-4 | 103.9 | 0.42 | 33 |
| MCZ-5 | 135.5 | 0.48 | 29 |

# Fig. 1

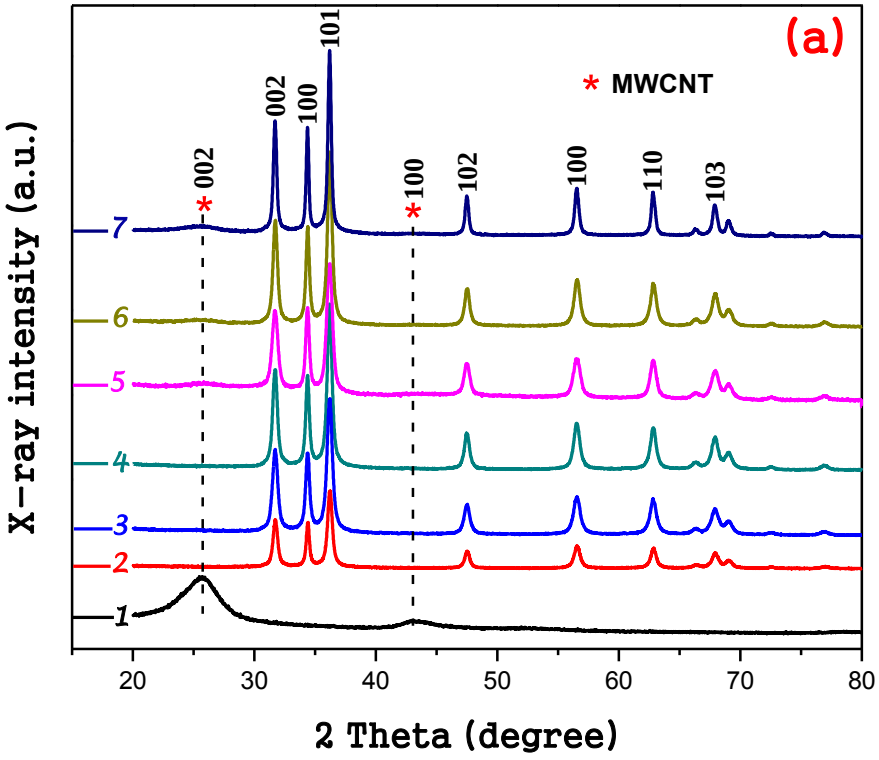
(a)
* MWCNT
002
100
101
* 002
* 100
102
100
110
103
7
6
5
4
3
2
1
X-ray intensity (a.u.)
20
30
40
50
60
70
80
2 Theta (degree)

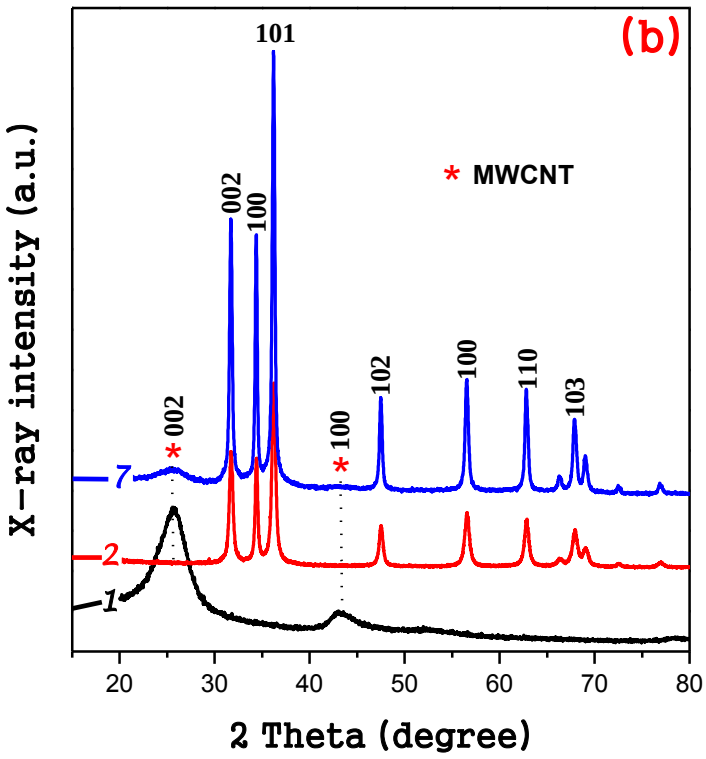
(b)
101
002
100
* MWCNT
* 002
* 100
102
100
110
103
7
2
1
X-ray intensity (a.u.)
20
30
40
50
60
70
80
2 Theta (degree)

# Fig. 2

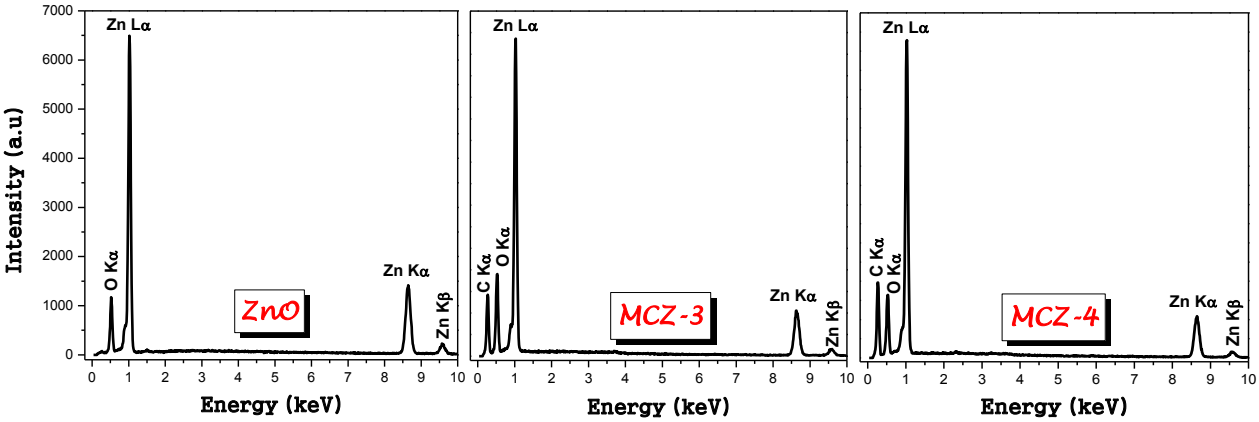

# Fig. 3

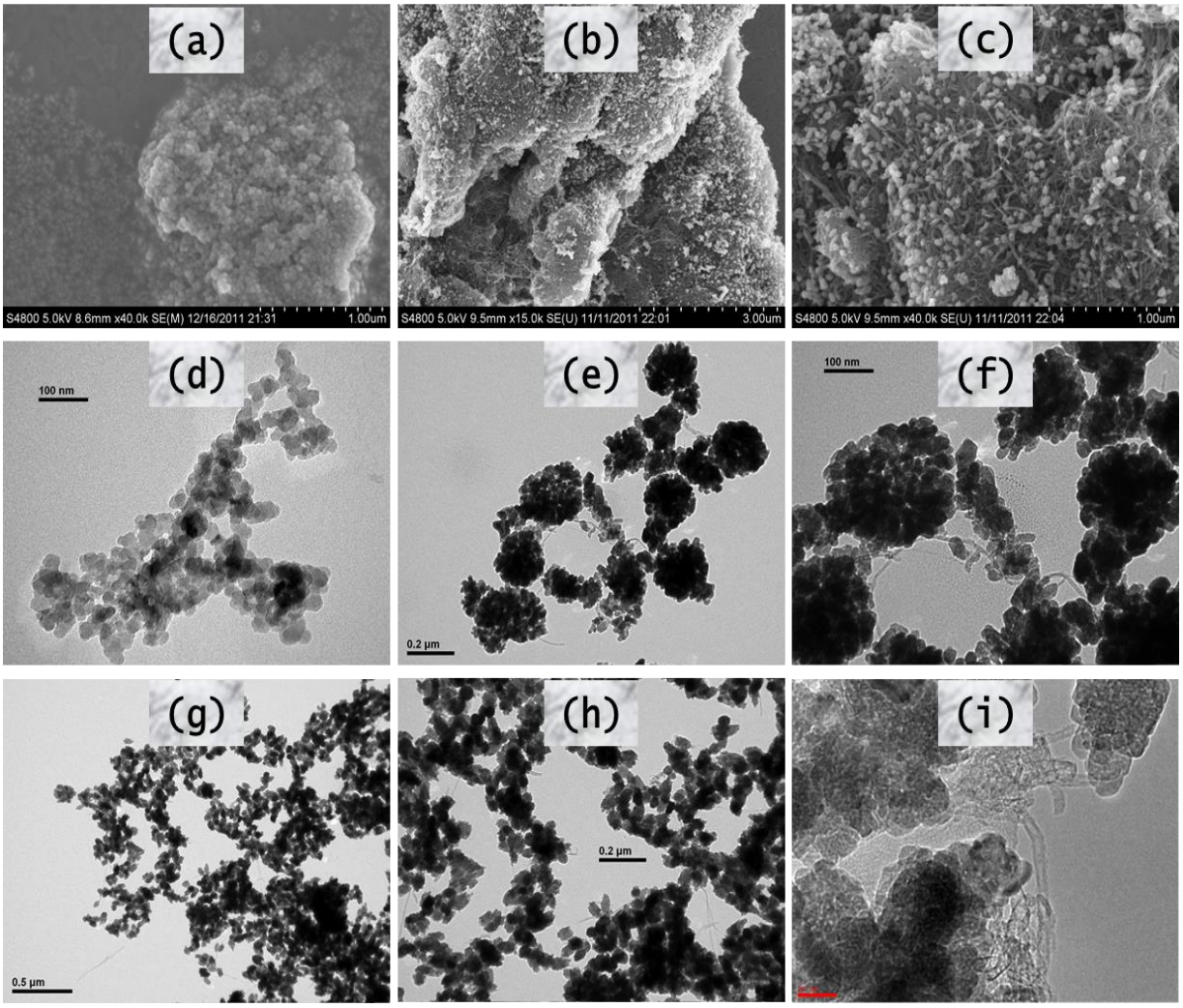
(a)
S4800 5.0kV 8.6mm x40.0k SE(M) 12/16/2011 21:31 1.00um
(b)
S4800 5.0kV 9.5mm x15.0k SE(U) 11/11/2011 22:01 3.00um
(c)
S4800 5.0kV 9.5mm x40.0k SE(U) 11/11/2011 22:04 1.00um
(d)
100 nm
(e)
0.2 μm
(f)
100 nm
(g)
0.5 μm
(h)
0.2 μm
(i)

# Fig. 4

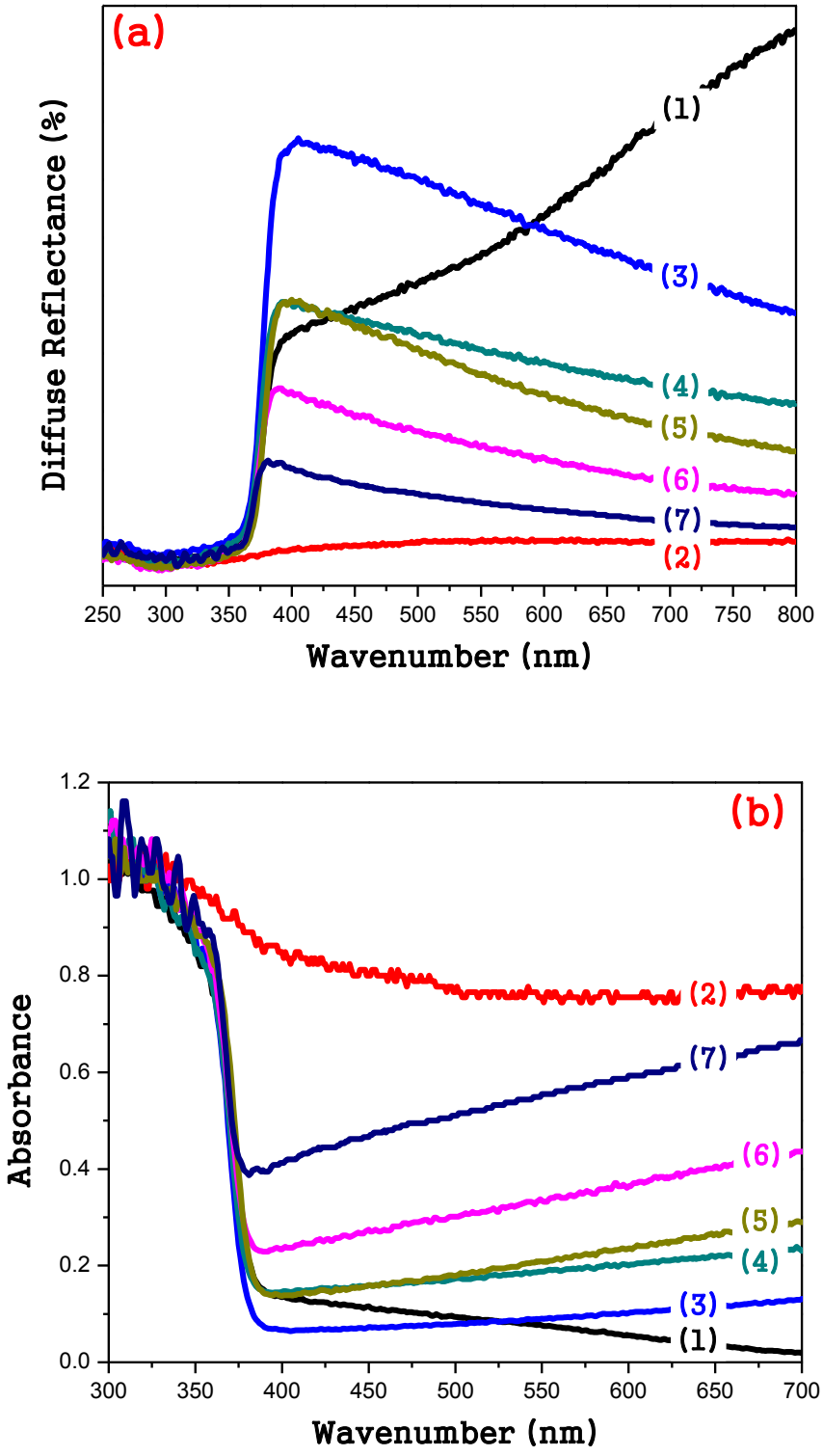
(a)
Diffuse Reflectance (%)
Wavenumber (nm)
250 300 350 400 450 500 550 600 650 700 750 800
(1)
(3)
(4)
(5)
(6)
(7)
(2)
(b)
Absorbance
Wavenumber (nm)
0.0 0.2 0.4 0.6 0.8 1.0 1.2
300 350 400 450 500 550 600 650 700
(2)
(7)
(6)
(5)
(4)
(3)
(1)

# Fig. 5

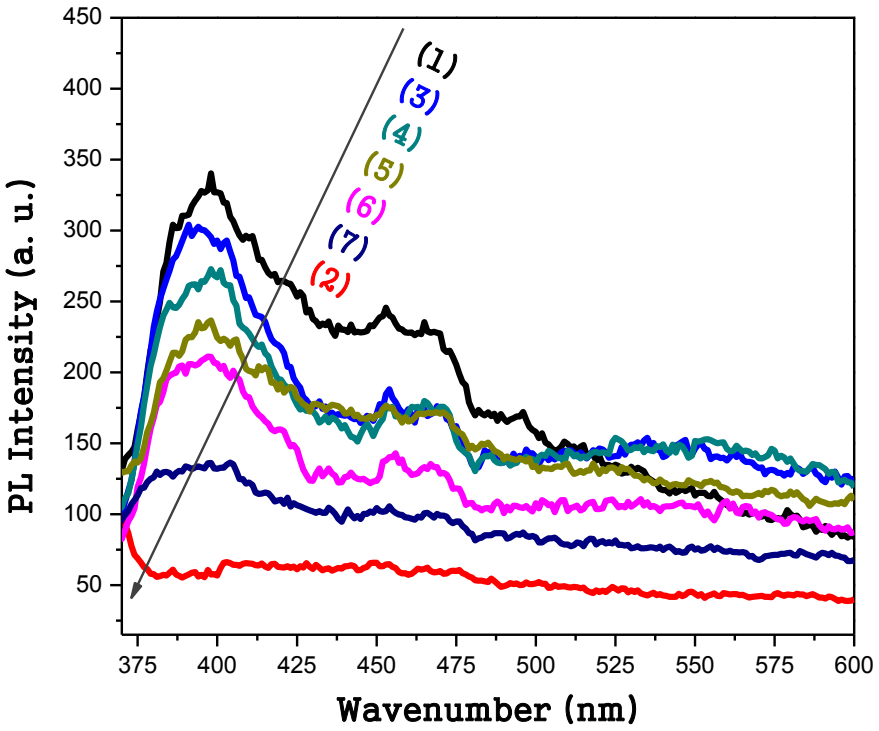
PL Intensity (a. u.)
Wavenumber (nm)
450
400
350
300
250
200
150
100
50
375
400
425
450
475
500
525
550
575
600
(1)
(3)
(4)
(5)
(6)
(7)
(2)

**Fig. 6**

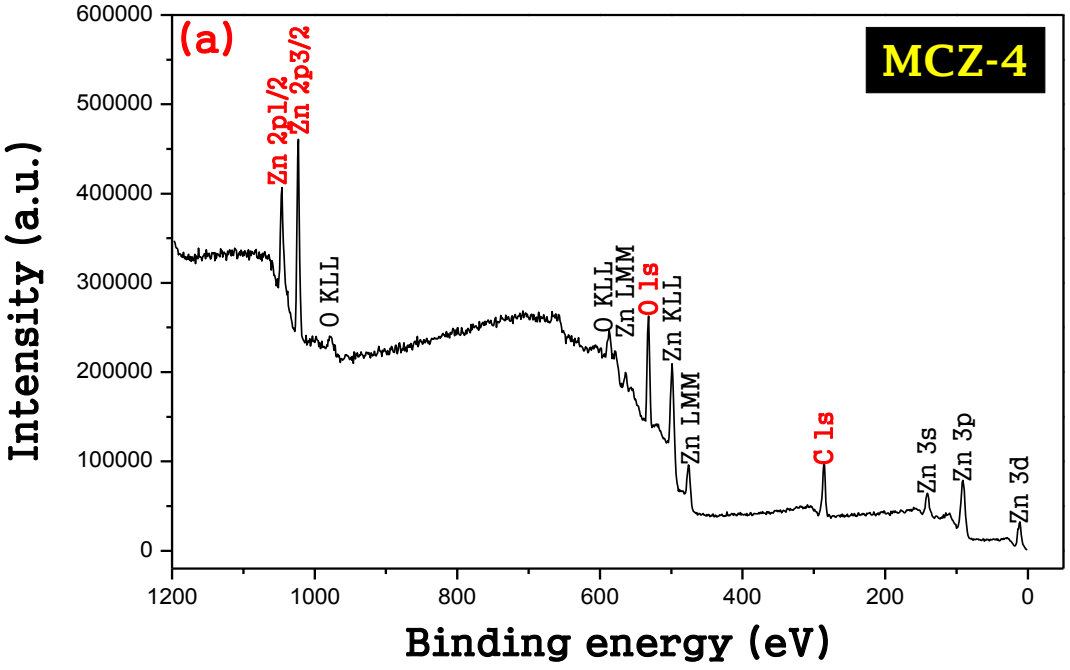
(a)
MCZ-4
Zn 2p1/2
Zn 2p3/2
O KLL
O KLL
Zn LMM
O 1s
Zn KLL
Zn LMM
C 1s
Zn 3s
Zn 3p
Zn 3d
Intensity (a.u.)
Binding energy (eV)
600000
500000
400000
300000
200000
100000
0
1200
1000
800
600
400
200
0

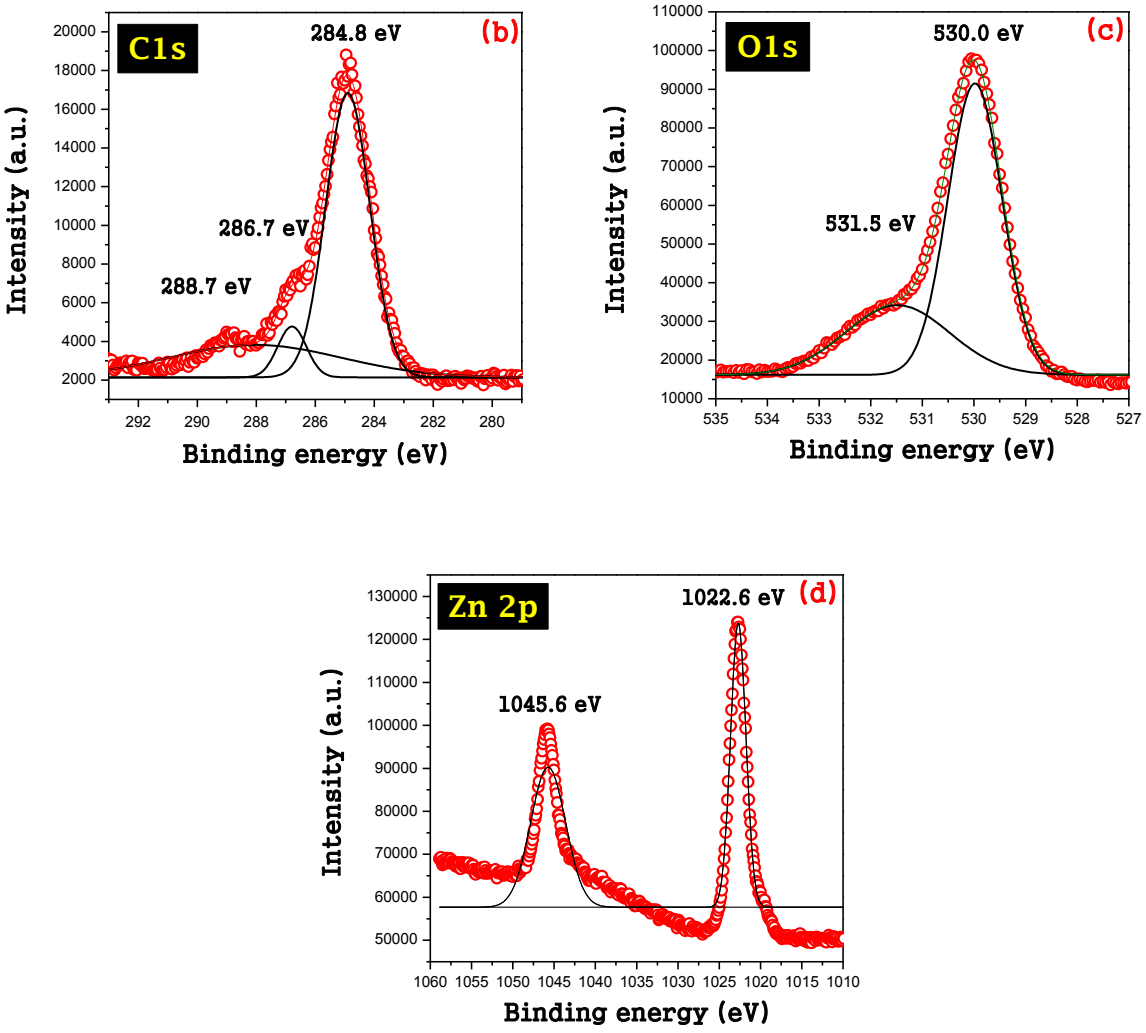
C1s
284.8 eV
(b)
286.7 eV
288.7 eV
Intensity (a.u.)
Binding energy (eV)
O1s
530.0 eV
(c)
531.5 eV
Intensity (a.u.)
Binding energy (eV)
Zn 2p
1022.6 eV
(d)
1045.6 eV
Intensity (a.u.)
Binding energy (eV)

# Fig. 7

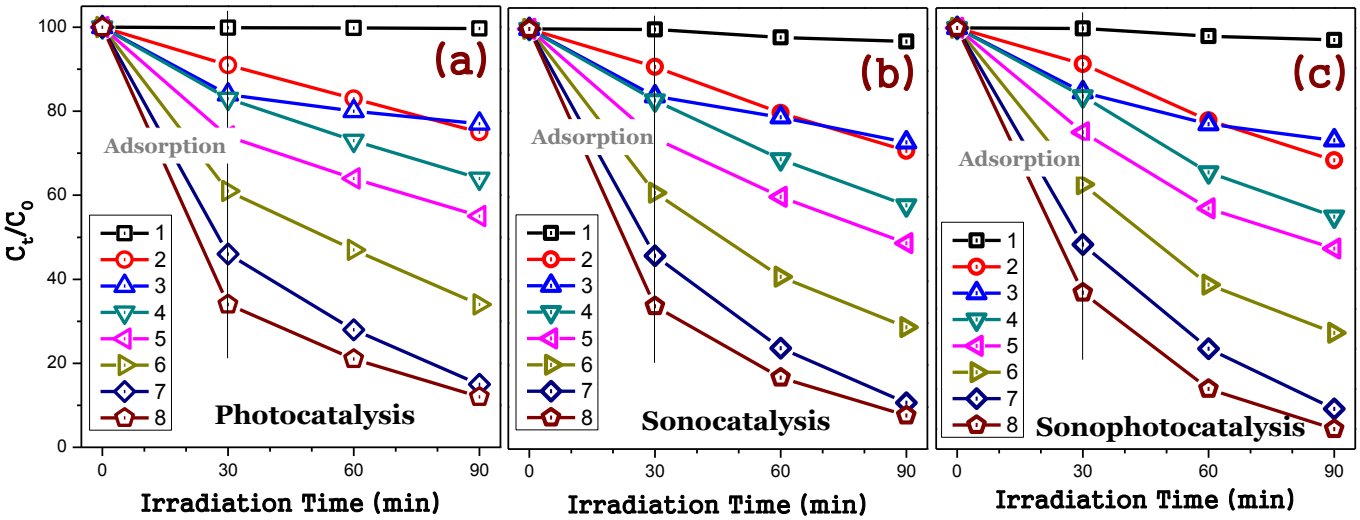
(a)
(b)
(c)
Adsorption
Photocatalysis
Sonocatalysis
Sonophotocatalysis
$C_t/C_o$
Irradiation Time (min)
0
20
40
60
80
100
0
30
60
90
1
2
3
4
5
6
7
8

# Fig. 8

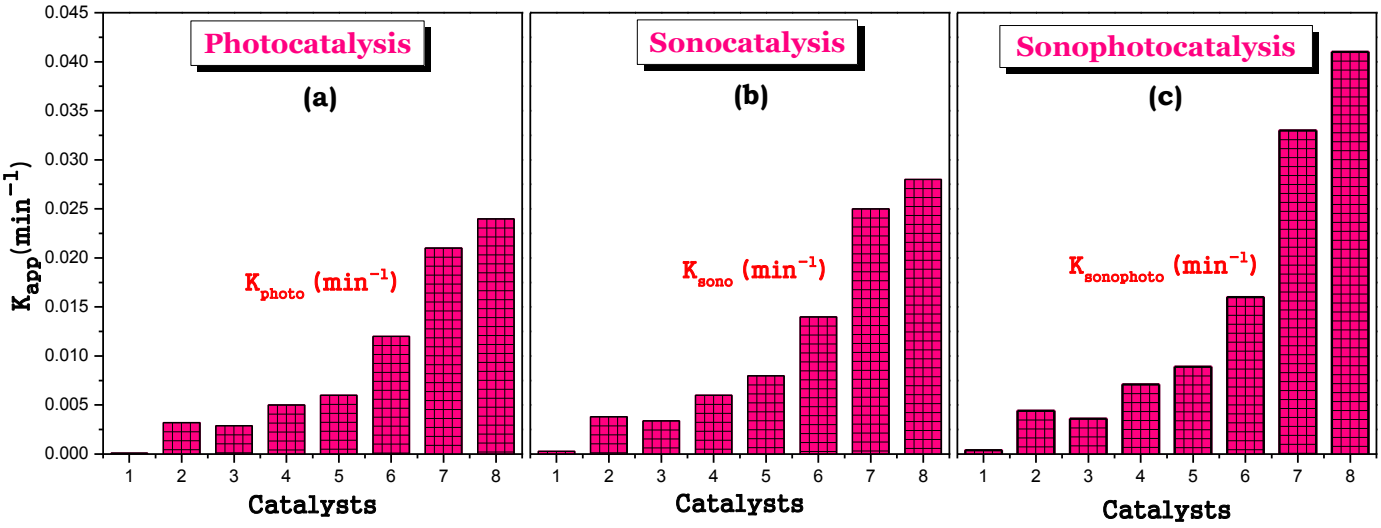
Photocatalysis
(a)
Sonocatalysis
(b)
Sonophotocatalysis
(c)
$K_{app}(min^{-1})$
$K_{photo}$ $(min^{-1})$
$K_{sono}$ $(min^{-1})$
$K_{sonophoto}$ $(min^{-1})$
0.045
0.040
0.035
0.030
0.025
0.020
0.015
0.010
0.005
0.000
1 2 3 4 5 6 7 8
Catalysts

# Fig. 9

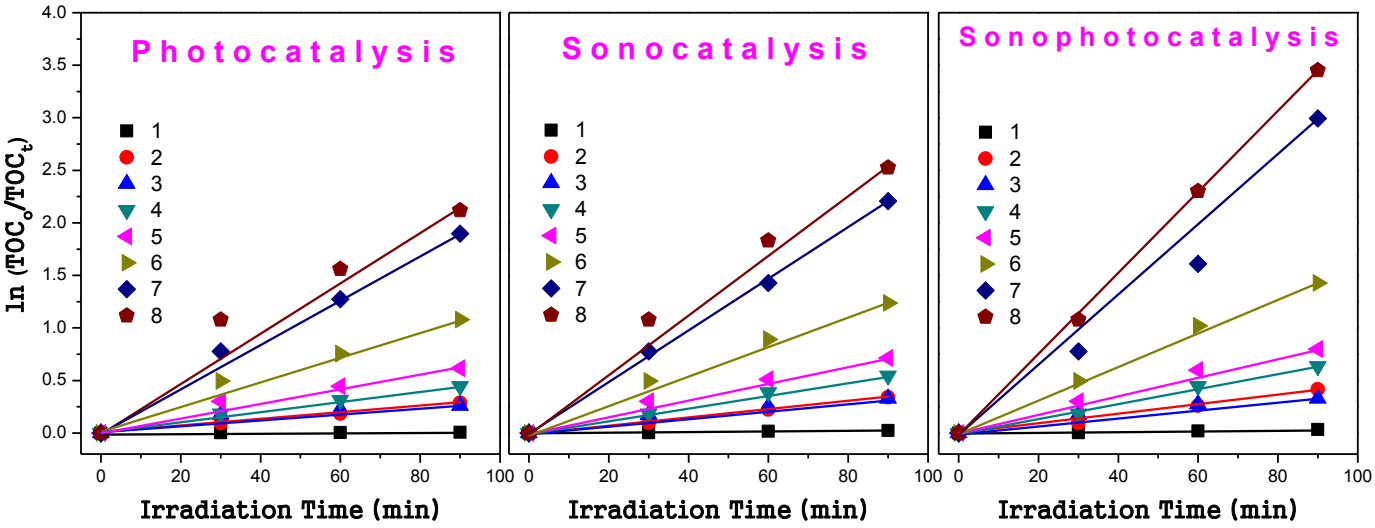
Photocatalysis
Sonocatalysis
Sonophotocatalysis
1
2
3
4
5
6
7
8
ln (TOC$_o$/TOC$_t$)
Irradiation Time (min)
0.0
0.5
1.0
1.5
2.0
2.5
3.0
3.5
4.0
0
20
40
60
80
100

# Fig. 10

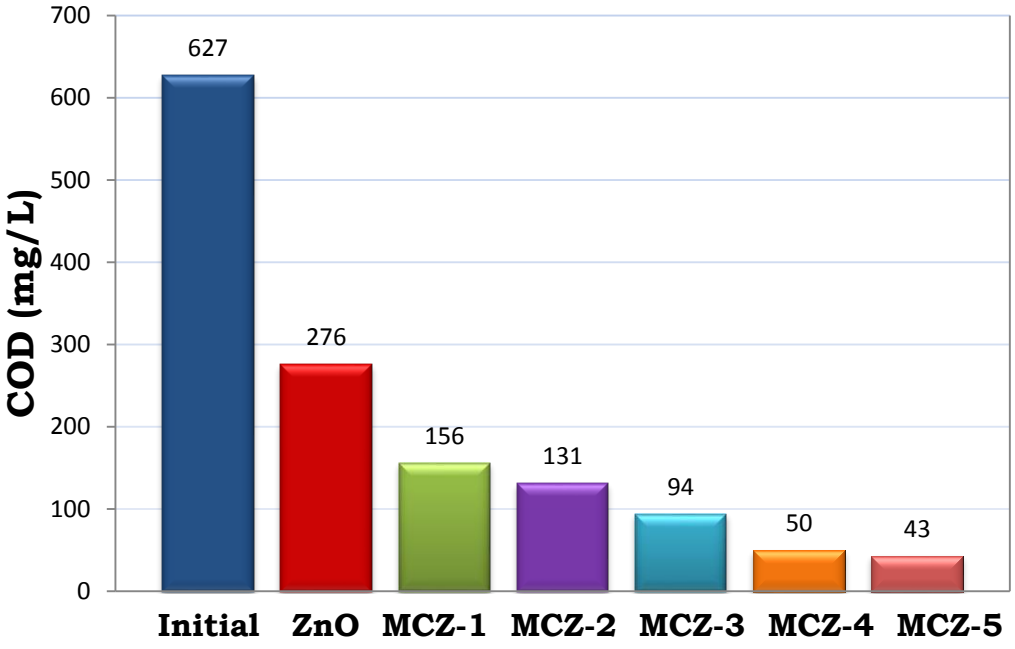
700
600
500
400
300
200
100
0
COD (mg/L)
627
276
156
131
94
50
43
Initial
ZnO
MCZ-1
MCZ-2
MCZ-3
MCZ-4
MCZ-5

# Fig. 11

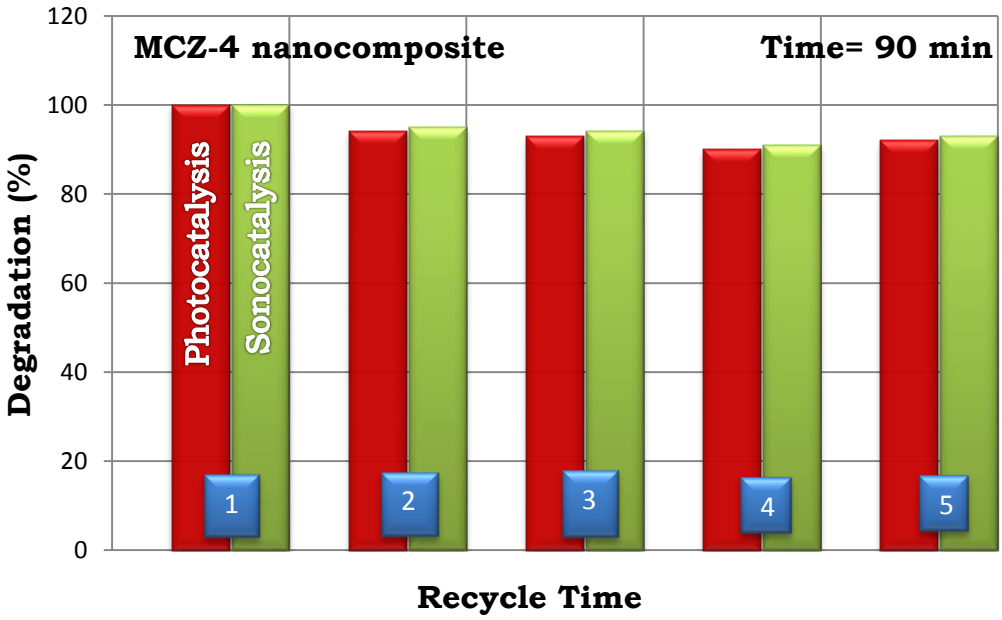
MCZ-4 nanocomposite
Time= 90 min
Degradation (%)
120
100
80
60
40
20
0
Photocatalysis
Sonocatalysis
1
2
3
4
5
Recycle Time